Journal of proteome research

Article

pubs.acs.org/jpr

PhosphoPath: Visualization of Phosphosite-centric Dynamics in Temporal Molecular Networks

Linsey M. Raaijmakers,[†,‡] Piero Giansanti,[†,‡] Patricia A. Possik,[§,∥] Judith Mueller,[§] Daniel S. Peeper,[§] Albert J. R. Heck,[†,‡] and A. F. Maarten Altelaar*[,†,‡]

[†]Biomolecular Mass Spectrometry and Proteomics, Bijvoet Center for Biomolecular Research and Utrecht Institute for Pharmaceutical Sciences, Utrecht University, Padualaan 8, 3584 CH Utrecht, The Netherlands

[‡]Netherlands Proteomics Center, Padualaan 8, 3584 CH Utrecht, The Netherlands

[§]Division of Molecular Oncology, The Netherlands Cancer Institute, 1066 CX Amsterdam, The Netherlands

Supporting Information

ABSTRACT: Protein phosphorylation is an essential post-translational modification (PTM) regulating many biological processes at the cellular and multicellular level. Continuous improvements in phosphoproteomics technology allow the analysis of this PTM in an expanding biological content, yet up until now proteome data visualization tools are still very gene centric, hampering the ability to comprehensively map and study PTM dynamics. Here we present PhosphoPath, a Cytoscape app designed for the visualization and analysis of quantitative proteome and phosphoproteome data sets. PhosphoPath brings knowledge into the biological network by importing publically available data and enables PTM site-specific visualization of information from quantitative time series. To showcase PhosphoPath performance we use a quantitative proteomics data set comparing patient-derived melanoma cell lines grown in either conventional cell culture or xenografts.

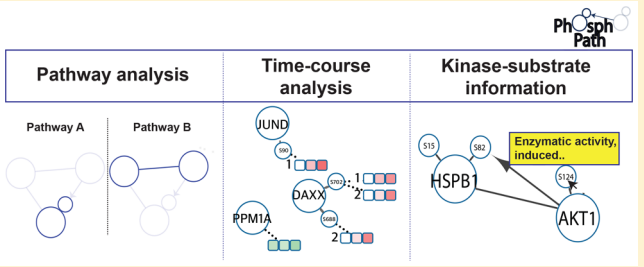

KEYWORDS: *posttranslational modifications, biological network analysis, phosphosite-centric dynamics, Cytoscape, signaling, phosphoproteomics, computational proteomics*

INTRODUCTION

Protein phosphorylation is one of the most studied post-translational modifications (PTMs) and plays an important role in biological processes. Phosphorylation can result in protein activation or repression and may affect protein stability, cellular localization, and interaction with binding partners. About 40% of human proteins are phosphorylated at any one time, and most proteins can be phosphorylated at multiple sites.[1,2] Recent technical advances in mass-spectrometry-based proteomics[3,4] and phosphopeptide enrichment[5] have increased the accessibility of this PTM, and an increasing number of phosphoproteomics studies are being performed.[6] Public databases such as PhosphoSitePlus,[7] phospho.ELM,[8] and Phosida[9] contain a large number of identified phosphorylation sites; however, the integration and representation of these data sets still lags behind compared with equivalent tools used for especially genomic and to a lesser extent protein-level based analysis. A recently published database for phosphorylation-mediated signaling networks, PhoSigNet,[10] attempted to tackle this problem by integrating data from different sources with additional information related to cancer. Although the database displays the currently available information related to pathways and kinase−substrate relationships, the network visualization is still not phosphosite-centric.

Current data analysis of a general phosphoproteomics experiment consists of multiple steps. After phosphopeptide identification and localization of the phosphorylated site, the phosphosites are quantified, potentially followed by normalization against protein expression levels when available.[11] The quantified phosphosites are further used for the analysis of differential regulation, followed by network analysis, which is mainly focused on protein−protein interactions. For network analysis, resources such as STRING[12] and Biogrid[13] are often used to extract protein interactions, followed by Kegg and Pathvisio[14] for pathway analysis. Information on kinase−substrate interactions is mainly retrieved from PhosphoSitePlus.[7] Although PhosphoSitePlus contains about 260 000 reported phosphorylation sites,[7] the function for most of these sites is not known nor is the responsible kinase. Because most proteins contain multiple phosphorylation sites, multiple kinases can be responsible for phosphorylating the same protein. To gain insight in this complexity, it is important to visualize these interactions in a phosphosite-specific manner. Currently available software tools lack this capability, including the PhosphoSitePlus Cytoscape app, which only visualizes

Received: June 8, 2015
Published: August 28, 2015

DOI: 10.1021/acs.jproteome.5b00529
J. Proteome Res. 2015, 14, 4332−4341

kinase−substrate interactions on the protein level rather than site-specific.

Besides the need for site-specificity, there is a need for visualizing time course data. To gain insight into the regulation of biological processes, one needs to monitor protein and PTM dynamics, requiring time-course experiments. Existing analysis software allows visualization of quantitative information but is limited in displaying multiple conditions or time points directly in the network.

In light of the huge interest in phosphoproteomics, large data availability, and the suitability of Cytoscape as a visualization platform, we developed PhosphoPath: a Cytoscape app for the visualization of phospho-site (and other PTM) centric data. PhosphoPath integrates data from three different public databases to identify protein−protein interactions and kinase−substrate interactions and performs pathway enrichment. Cytoscape[15] is a widely used open-source tool for the visualization and exploration of biological interaction networks, which freely can be extended with plugins ("apps" in Cytoscape nomenclature) to add diverse functionalities including enrichment analysis, data integration, and online data import. A large collection of these apps is available via the integrated "app store",[16] but these presently focus almost exclusively on genomics-oriented data, hampering analysis of phosphorylation dynamics. There is thus currently a need for PTM site-specific software tools suited for the exploration of phosphoproteomic data sets.

In the here presented PhosphoPath suite, interactions are visualized on both the level of protein−protein interactions and site-specific for kinase−substrate interactions. Moreover, quantitative information for multiple conditions or time points can be displayed at both levels. Networks can be expanded with missing interacting proteins extracted from databases. Although PhosphoPath is largely focused on phosphoproteomics data, it is also possible to include different types of PTMs. When different modification types are imported, the visualizations can be customized for each type. Information available for specific PTM sites such as the biological process, function, effect on protein stability, and so on is all loaded in the network.

To demonstrate the broad potential of PhosphoPath, we used data from a comprehensive proteome and phosphoproteome analysis of the phosphorylation driven signaling events in BRAF mutant melanoma, resulting in the activation of the mitogen-activated protein kinase (MAPK) pathway.[17] The inhibitors that specifically target the mutated form of BRAF—vemurafenib[18] and dabrafenib[19]—show initial tumor response; however, resistance develops after 5−7 months.[18,20,21] Despite a number of studies focusing on this problem,[22,23] still no single or combination treatment has been able to completely overcome the resistance in BRAF melanoma, in part caused by a disconnect between the in vitro (cell-culture-based) model systems used for initial drug screening and human physiology.[24] For this reason, more in-vivo-like model systems such as tumor xenografts are increasingly used, and here we investigate differential phosphorylation dynamics of melanoma cells grown in either conventional cell culture or tumor xenografts and use PhosphoPath to mine the data and visualize signaling events.

METHODS

Sample Preparation for MS

Human melanoma cell line 888MEL was cultured in DMEM supplemented with 9% FBS (Sigma), 2 mM glutamine, 100 U/mL penicillin, and 0.1 mg/mL streptomycin (all Gibco). For the xenograft experiment, 5×10^5 cells were embedded 1:1 in medium and growth-factor-reduced matrigel (BD Biosciences) and injected subcutaneously into the flank of NSG (NOD.Cg-Prkdcscid Il2rgtm1Wjl/SzJ) mice (the Jackson laboratory). Tumor growth was monitored by calipering. 1, 2, and 3 weeks after injections, animals were euthanized, and tumors were removed for protein extraction. Animal experiments were performed following local and international regulations and ethical guidelines and have been authorized by the local experimental animal committee at The Netherlands Cancer Institute.

Tumor samples were fixed in ethanol/acetic acid/formol saline fixative (EAF) (40:5:10:45 v/v), embedded in paraffin, and stained with hematoxilin/eosin according to common procedures (Supplementary Figure 4).

Subsequently, melanoma cells and xenograft tumors (i.e., week1, week2, and week3) were lysed on ice by sonication after dounce homogenization in buffer containing 50 mM ammonium bicarbonate (pH 8.0), 8 M urea, 1 mM sodium orthovanadate, complete EDTA-free protease inhibitor mixture (Roche), and phosSTOP phosphatase inhibitor mixture (Roche). Lysates were then clarified by centrifugation at 20,000*g* for 15 min at 4 °C. The total protein concentration was determined using a Bradford Assay (BioRad). Total protein lysate from each condition (∼1 mg) was reduced with DTT at a final concentration of 4 mM at 56 °C for 25 min; subsequently, samples were alkylated with iodoacetamide at a final concentration of 8 mM at RT for 30 min in the dark. Proteins were then digested using Lys-C (enzyme/substrate ratio 1:100, Wako) and incubated for 4 h at 37 °C. The solution was then diluted to a final urea concentration of 2 M with 50 mM ammonium bicarbonate, and trypsin was added (enzyme/substrate ratio 1:100, Promega) and incubated at 37 °C overnight. The digestion was quenched by acidification to 5% formic acid. Resulting peptides were then chemically labeled with stable isotope dimethyl labeling using a Sep-Pak C18 column (Waters) as previously described.[25] Equal amounts of protein sample were labeled on-column using "light", "intermediate", and "heavy" dimethyl labeling reagents. For the first replica, the light label (L) was used for the 888Mel cell line, while the intermediate (I) and heavy dimethyl labels (H) were used for the xenograft tumors after 1 and 2 weeks, respectively. In the second replica the light label was used for the 888Mel cell line, while the intermediate and heavy dimethyl labels were used for the xenograft tumors after 2 and 3 weeks, respectively. The resulting solution was then dried in vacuo and stored at −80 °C.

The differently dimethyl-labeled peptides were subsequently reconstituted in 10% formic acid and mixed in 1:1:1 ratio for each experiment prior to fractionation using strong cation exchange (SCX) and Ti^{4+}-IMAC phosphopeptide enrichment as previously described.[26]

Mass Spectrometric Analysis

After reconstituting the enriched phosphopeptides (24 enrichment for each replica) in 10% formic acid, phosphopeptides were subjected to a reversed phase nano-UHPLC−MS/MS analysis consisting of a Proxeon EASY-nLC 1000 (Thermo Scientific) connected to a LTQ-Orbitrap Velos or Elite (Thermo Scientific). The injected sample was first trapped with a double-fritted trapping column (Dr Maisch Reprosil C18, 3 μm, 2 cm × 100 μm) at a maximum pressure of 800 bar

DOI: 10.1021/acs.jproteome.5b00529
J. Proteome Res. 2015, 14, 4332−4341

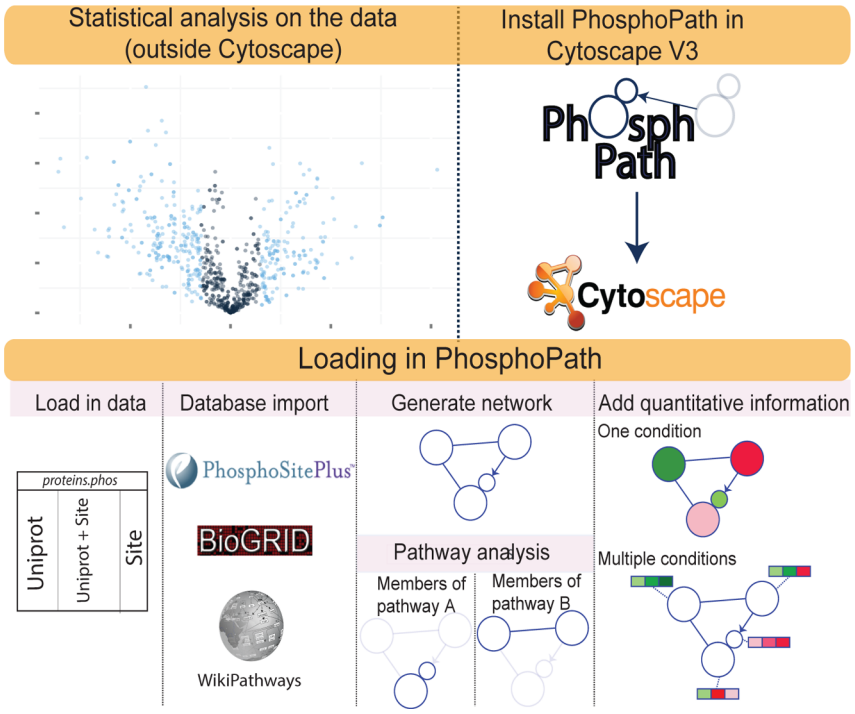

Figure 1. Example workflow for the network visualization of phosphosite-centric dynamics using PhosphoPath. Differential expressed proteins/phosphosites are preferably identified using a user-defined statistical test, followed by analysis in Cytoscape. The list of differential expressed entries is imported as well as publically available data from PhosphoSitePlus, Biogrid, and Wikipathways for the generation of a protein−protein interaction network and pathway analysis. Quantitative information can be added to the network to visualize dynamics of the acquired network.

with 100% solvent A (0.1% formic acid in water) before being separated on the analytical column (either Agilent Poroshell 120 EC-C18, 2.7 μm, 40 cm × 50 μm or Agilent Zorbax SB-C18, 1.8 μm, 40 cm × 75 μm). Peptides were chromatographically separated by a 60, 90, or 150 min gradient, consisting of 7 to 30% solvent B (0.1% formic acid in ACN) at a flow rate of 150 or 100 nL/min. The total measurement time for the different gradients was 90, 120, or 180 min. The eluent was sprayed via a distal-coated fused silica emitter (360 μm o.d., 20 μm i.d., 10 μm tip i.d.; constructed in-house) butt-connected to the analytical column. The ion spray voltage was set to 1.7 kV.

The LTQ-Orbitrap Velos and Elite mass spectrometers were operated in a data-dependent mode to automatically switch between MS and MS/MS. In brief, survey full-scan MS spectra were acquired in the Orbitrap scanning from m/z 350 to m/z 1500 at a resolution of 60 000 at m/z 400 using an AGC setting of 1×10^6 ions. Charge-state screening was enabled, and precursors with unknown charge state or a charge state of 1 were excluded. After the survey scans, the 10 or 20 most intense precursors were selected for subsequent HCD or ETD-IT fragmentation. A programmed data-dependent decision tree determined the choice of the most appropriate technique for a selected precursor.[27] In essence, doubly charged peptides were subjected to HCD fragmentation, and more highly charged peptides were fragmented using ETD. The normalized collision energy for HCD was set to 35%. Supplemental activation was enabled for ETD. Dynamic exclusion was enabled (exclusion size list 500, exclusion duration 30, 40, or 60 s).

Data Processing

Each raw file was processed and quantified with MaxQuant version 1.4.1.2.[28] All raw files were searched against a Swissprot database version 2012_09 with taxonomy either *Homo sapiens* (20 235 sequences) or *Mus musculus* (16 570 sequences). The database search was performed with the following parameters: up to two missed cleavages and cysteine carbamidomethylation as fixed modification. Light, intermediate, and heavy dimethylation of peptide N-termini and lysine residues; methionine oxidation; protein N-terminal acetylation; and STY phosphorylation were set as variable modifications. The enzyme was specified as trypsin. For all experiments only unique peptides were considered for protein quantification, and unique mouse proteins were considered as contaminants and therefore were removed for the further analysis. Protein and PSM FDR were set to 0.01; the delta score for modified peptides was kept at the default value of 17. Only class I phosphorylation sites (localization probability $p > 0.75$) were taken further in the analysis. The median Log_2 ratio and median absolute deviation (MAD) of all quantified proteins were used to determine significant regulation. Because of the limited number of replicates and to decrease the risk of including false-positives, a more stringent cutoff of 2 fold was chosen for further analysis of significant up- and down-regulated proteins and phosphosites in PhosphoPath.

RESULTS

PhosphoPath Development

PhosphoPath is developed as app for Cytoscape 3 built on top of the Open Service Gateway Initiative (OSGI) to analyze mouse, human or rat data sets. A manual with example data sets is made available at https://github.com/linseyr/PhosphoPath/ and the cytoscape app store. By loading this app into Cytoscape the user can analyze data on pathway enrichment, protein−protein interactions, and quantitative changes (Figure 1). The input for this app can contain both quantitative data on identified proteins as well as phosphorylation sites and can also

DOI: 10.1021/acs.jproteome.5b00529
J. Proteome Res. 2015, 14, 4332−4341

accommodate other PTMs (e.g., acetylation, methylation). When proteins are imported as Uniprot IDs, PhosphoPath will automatically convert the ids to gene symbols for uniform visualization purposes. Combining proteome with phosphorylation status gives a more complete overview of upstream and downstream regulation.

To demonstrate the functionalities of PhosphoPath, we have used a comprehensive quantitative proteomics data set containing information on both protein expression and phosphosite-centric abundance. This data set was derived from the melanoma cell line 888MEL grown either in conventional cell culture or as tumor xenograft; therefore, this system should reveal the differences in tumor growth under in vitro and in vivo conditions. The tumor xenograft model is derived from transplantation of human melanoma cells under the skin of an immune-compromised mouse to avoid rejection of the human cells. The tumor develops in several weeks, and tumor progression can be studied in this model organism in vivo. Here xenografts were grown for 1, 2, or 3 weeks before samples were collected to allow the drafting of temporal phosphorylation dynamics in an expanding tumor. The phosphorylation status of these xenograft tumors was compared with the same cell line in conventional cell culture, in two quantitative experiments comparing cell culture to week 1 and 2 or week 2 and 3, respectively (Figure 2A).

Processing the Data

All at least 2-fold up- and down-regulated proteins and phosphosites were used for analysis in PhosphoPath (Figure 2B). To identify interacting partners and calculate pathway enrichment we have used the PhosphoPath import option to retrieve the most up-to-date information from (1) PhosphoSitePlus,[7] (2) Biogrid,[13] and (3) Wikipathways.[29] PhosphoSitePlus is an open, manually curated resource for PTMs, containing ~450 000 modification sites. By selecting this database, updated kinase and substrate data are imported, and interactions are visualized by an arrow from kinase to specific phosphorylation site (Figure 3A). All available information about the process and function of a phosphorylated site can be visualized by placing the mouse cursor over the specific site in the network (Figure 3B). This information is also stored in the node table, to allow for filtering on specific processes or functions for phosphorylation events. Biogrid (Biological General Repository for Interaction Data sets) is an open resource for curated physical and genetic interactions. Selecting this database imports the latest release of interaction data identified from various experimental methods. After the data are imported, interactions are visualized in the network by a straight line between the protein nodes. The visual style in the network, like the edge color or thickness, can be adjusted at the users discretion to distinguish between interaction types, like physical, transient, or genetic interaction. Besides Biogrid, users can choose to import their own interaction data set in tab-delimited format (e.g., from alternative databases such as STRING). This interaction data can be imported on top of the Biogrid data or independently. The source of the interaction is saved in the edge table and can later be used to distinguish between interactions retrieved from Biogrid and user-defined interactions. The last data source, WikiPathways, is used for pathway analysis. Wikipathways is an open, collaborative biological pathway database that provides fully annotated pathway diagrams. By selecting this database, the proteins in the data set are queried against the database to identify the

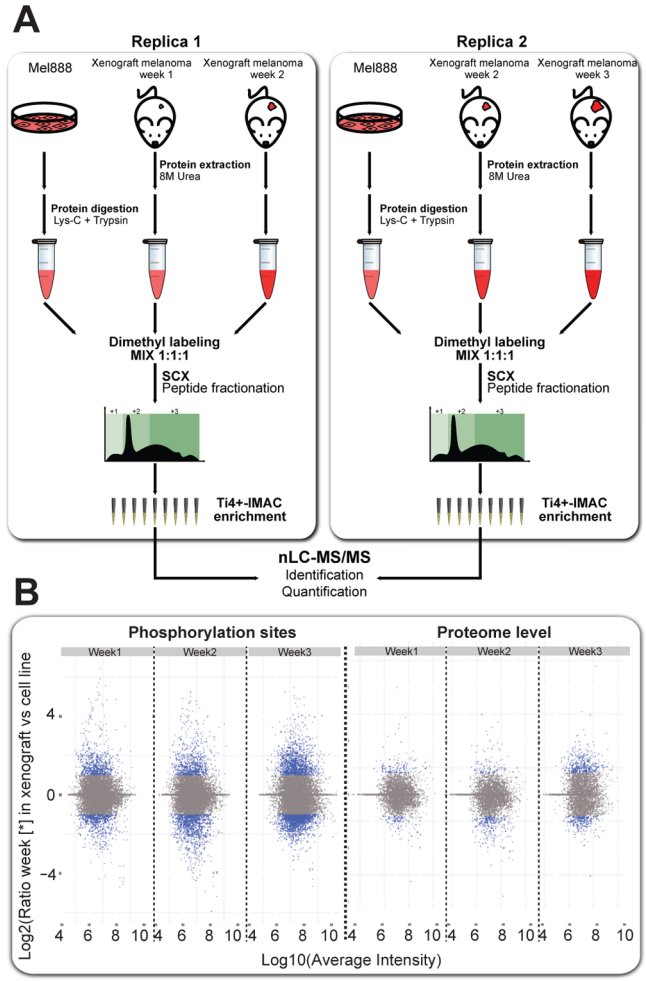

Figure 2. Phosphoproteomics workflow (A) and resulting MA plots (B) used to profile phosphoproteome dynamics during melanoma xenograft growth. (A) Lysates originating from in vitro and in vivo samples were digested into peptides using a tandem digestion with Lys-C and trypsin. Peptides were differentially labeled with three stable-isotope dimethyl labels and subsequently combined in a 1:1:1 ratio, followed by fractionating using strong cation exchange (SCX). The SCX fractions were desalted and pooled into 24 discrete samples, which were then enriched for phosphopeptides by Ti^{4+}-IMAC. All of the (phospho)peptide mixtures were analyzed via nano-LC–MS/MS. (B) MA plots phosphorylation sites and proteome, respectively. Log10 of the average intensity was plotted against the log2 ratio of week1, week2, and week3 against cell line. The median Log_2 ratio and median absolute deviation (MAD) of all quantified proteins were used to determine significant regulation. Proteins and phosphorylation sites with a log2 ratio >1 and < −1 were used for analysis and are colored in blue.

pathways they are involved in. To provide information about the representation of these pathways across the data set, we calculated enrichment using the Fisher exact test.[30] The total list of identified proteins from both the proteome and phosphoproteome experiments was used as background to calculate pathway enrichment of the regulated sites/proteins. *P* values from this enrichment test are corrected for multiple testing by Benjamini–Hochberg correction.[31]

Network Visualization

After importing all relevant information, networks can be visualized for pathways of interest. All pathways containing at least one protein are ordered based on their enrichment *p*

DOI: 10.1021/acs.jproteome.5b00529
J. Proteome Res. 2015, 14, 4332–4341

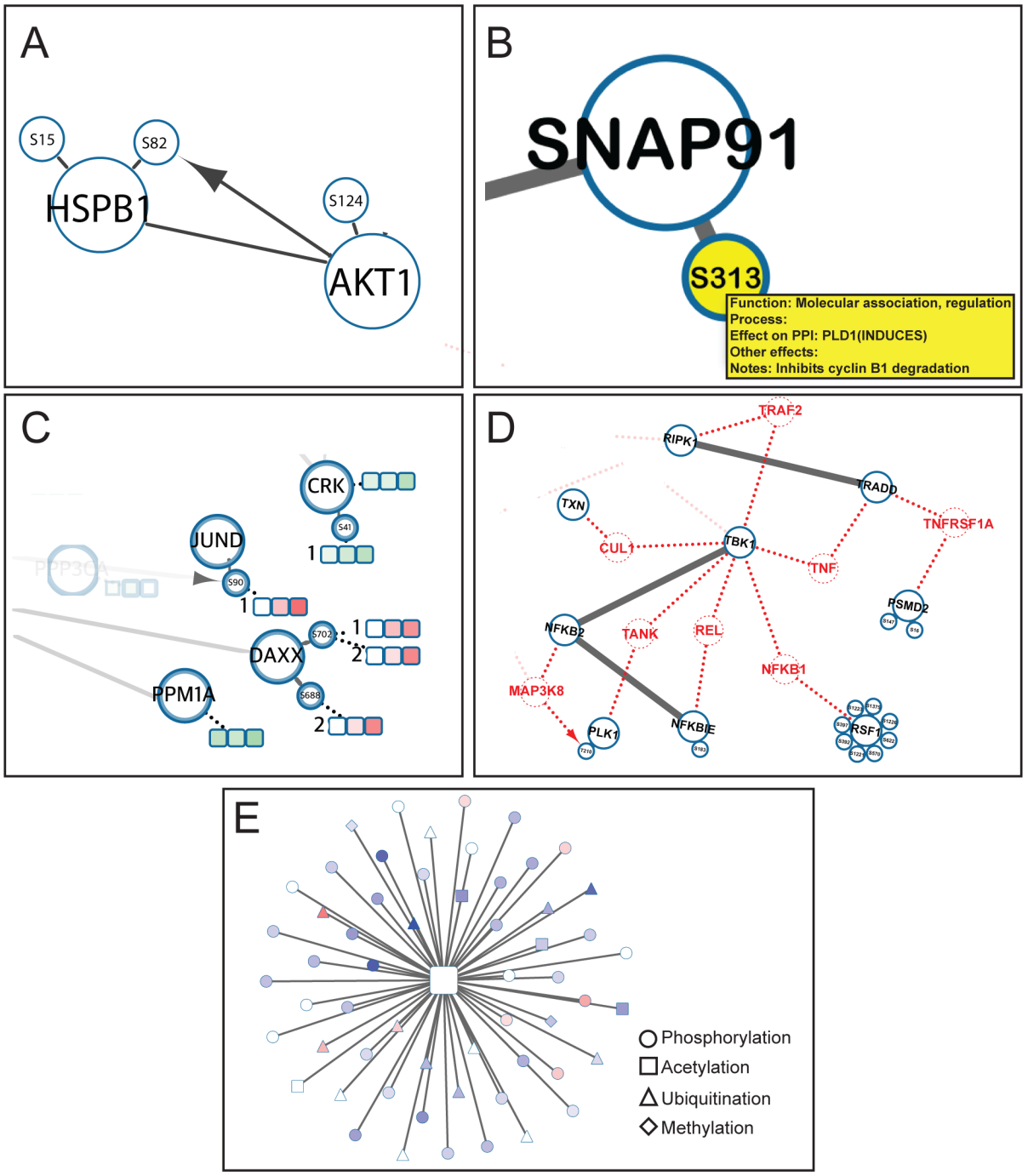

Figure 3. Functionalities of PhosphoPath. (A) Kinase−substrate interactions are visualized by an arrow from the kinase protein to its phosphorylation site on the substrate. (B) Available information from PhosphoSitePlus is visualized when the mouse cursor is placed on the specific site. (C) Quantitative information can be added to the network for several time points or conditions. The user specifies the number of conditions, and PhosphoPath will visualize this by a color bar. The color scheme can be adjusted by the user and represents the quantitative information for multiple conditions. Phosphorylation sites quantified on singly phosphorylated peptides or multiply phosphorylated peptides can be distinguished by the multiplicity described in front of the color bar. (D) The network can be enlarged with interacting proteins found in PhosphoSitePlus and Biogrid or the user-defined interaction data set. When a protein can link two proteins in the network together by a protein−protein interaction, it will be added to the network. The edge between this newly added protein and the proteins in the network is colored red. The user can also manually add a selected protein to the network. Interactions from the databases will then automatically be added to the network. (E) Visualization of different types of PTMs in one network. The shape of the nodes is adjusted to the type of modification, and the fill color represents the quantification.

value, with the most enriched pathways on top of the table. When one or multiple pathways are selected, PhosphoPath allows representation of subnetworks, containing proteins present only in the selected pathways. Among the top regulated pathways between xenograft and cell line we identified the focal adhesion pathway, cell cycle, MAPK signaling, and the EGFR signaling pathway. These pathways are previously described as deregulated in many cancers. Comparison of the activation of these selected pathways in cells derived from the same patient but grown either in conventional cell culture or as xenograft

DOI: 10.1021/acs.jproteome.5b00529
J. Proteome Res. 2015, 14, 4332−4341

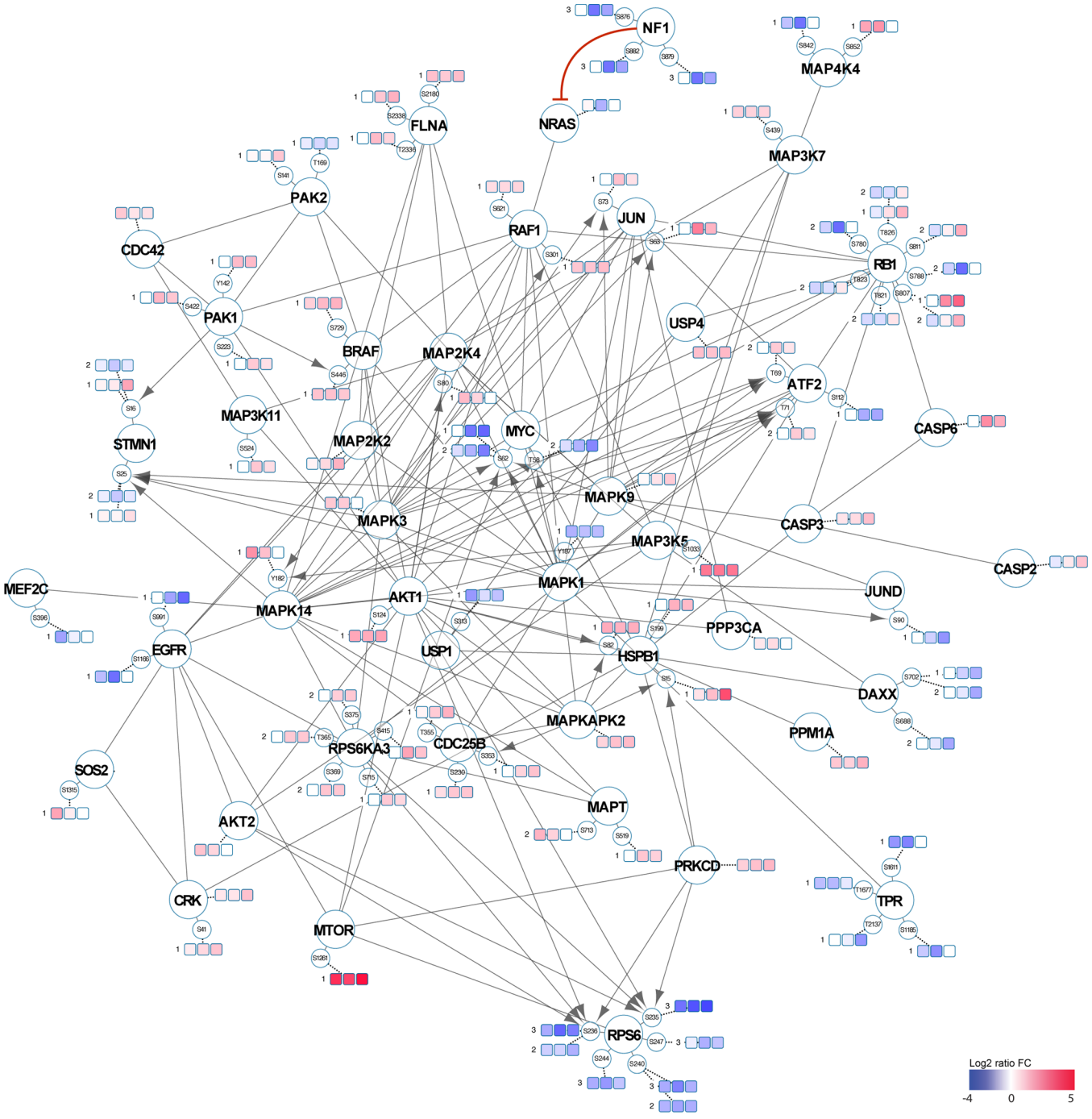

Figure 4. Interaction network of members of the MAPK pathway. Quantitative information for three comparative conditions (week1/cell line, week2/cell line, week3/cell line) is added to the network. The blue color represents down regulation and red up regulation. A straight line visualizes protein−protein interactions from Biogrid, and kinase−substrate interactions from PhosphoSitePlus are visualized by an arrow. The red edge is manually added to the network and shows inhibition from NF1 on NRAS. Multiplicity of the quantified peptide is visualized in front of the color bar.

clearly shows differential regulation. A likely explanation is the 3-D environment of the xenograft model system that causes this discrepancy, where pathways are regulated by signals from neighboring tumor cells as well as tumor surrounding cells, which are absent in conventional cell culture, limiting cell-to-cell communication.

Since the discovery of the BRAF mutation in melanoma in 2002, the RAS-RAF-MEK-ERK1/2 pathway, part of the MAPK cascades, attracted most attention. This pathway is involved in cell proliferation and survival and is deregulated in many cancers. Up to 90% of melanomas show activation of ERK due to mutations in BRAF and NRAS and stimulation of growth factor receptors such as HGFR and FGFR.[32] Because of the importance of this pathway we used PhosphoPath to analyze this further. By adding quantitative information on different experimental conditions we can monitor the progression of activation states. In the MAPK pathway we found 57 proteins regulated at the protein or phosphorylation level. With PhosphoPath we can now display the identified phosphosites on top of the protein information and add quantitative

DOI: 10.1021/acs.jproteome.5b00529
J. Proteome Res. 2015, 14, 4332−4341

information by a color bar representing the number of quantified conditions (any number larger than 1, Figure 3C). In this study we have data from four experimental conditions, allowing three quantitative comparisons (cell culture versus xenografts grown for 1 week, 2 weeks, or 3 weeks). For each entry we added a color bar representing the log 2 fold change of the three comparisons for the phosphoproteomics data. Combining the quantitative information for both protein and phosphorylation level can be used to distinguish increase in phosphorylation from increased protein expression, such as in the case of CRK, showing an increase in phosphorylation state equal to the increase in CRK protein expression (Figure 3C).

A common problem in visualization of these data sets is the presence of quantitative data for multiply phosphorylated peptides. When phosphorylation sites are close together in the protein, they could end up being quantified on the same peptide. In this case the quantification is not specific to that particular site but to the combination of those sites. Such peptides can be observed as singly phosphorylated on either of the two potential sites or doubly phosphorylated, leading to multiple quantification results for the same peptide sequence. An added benefit of using PhosphoPath is that it tackles this problem by visualizing all quantification results and adding the multiplicity in which the phosphorylation sites are quantified. This is exemplified in Figure 3C, where the phosphorylation site DAXX-S702 is quantified as a single phosphorylation event and as a double phosphorylation together with DAXX-S688.

PhosphoPath also provides the option to enlarge the network with interacting proteins from Biogrid and PhosphoSitePlus. When a protein in these databases can link proteins in the network together via protein−protein interactions or kinase-substrate interactions, it will be placed in the network (Figure 3D). These added proteins are displayed using an alternative color and are connected through dotted lines, to be able to distinguish them from the original experimentally derived proteins. The addition of such theoretical interactors can be performed in multiple rounds, with each round increasing the size of the network. It is also possible to import proteins defined by the user, after which all known interactions with the newly added proteins will be included in the network from Biogrid and PhosphoSitePlus.

Case Study

When comparing the xenograft model versus cell line we were able to identify regulation in several pathways, among which the MAPK pathway (Figure 4), focal adhesion pathway (Supplementary Figure S1), and WNT signaling (Supplementary Figure S2). Data visualization using PhosphoPath shows regulation of both the protein and phosphosite level. In the MAPK interaction network in Figure 4 we see an up-regulation of CDC42 on the protein level. CDC42 is a small GTPase of the Rho family, involved in cell morphology, migration, endocytosis, and cell cycle progression and is known to bind to PAK1. This binding leads to a conformational change of PAK1, followed by autophosphorylation and activation.[33] PAK1 is often found up-regulated in cancer and promotes tumor growth[34,35] and is activated by interaction with CDC42[36] or by phosphorylation.[33] As expected, the network shows an up-regulation of the phosphorylation state of PAK1 on multiple sites as well as for its downstream substrates BAD, BRAF, and STMN1. STMN1 was recently identified as a potential oncogene in melanoma by increasing cell proliferation and migration.[37] The phosphorylation dynamics of STMN1 in the MAPK pathway show a decrease in the doubly phosphorylated peptide at side S16 and S25, while abundances of both single sites increase, providing an interesting example of the capabilities of PhosphoPath to distinguish multiple forms of the same phosphosite. Spectra for doubly and singly phosphorylated peptides are shown in Supplementary Figure S3.

We further see deregulation of multiple sites at NF1. NF1 is a tumor suppressor with an important role in preventing melanoma initiation and progression and resistance to therapy.[38,39] Loss of NF1 function releases the negative regulation of RAS, resulting in increased signaling through downstream pathways, including the PI3K/AKT and the MAPK signal transduction cascades.[40] In this case we see a decrease in the phosphorylation level of NF1, leading to NF1 activation and NRAS inhibition (manually added to the MAPK network in red; Figure 4). Downstream of NRAS, we see increased phosphorylation of RAF1 on Serine 301, leading to RAF1 inactivation. This inactive state is maintained by phosphorylated S621 that functions as a binding site for 14−3−3 proteins and leads to further inactivation of the MAPK pathway.[41] Most regulation at phosphorylation level is seen on RB1 and RPS6. RB1 is important for its role in cell cycle progression. Phosphorylated RB1 releases E2F and induces expression of target genes leading to progression from G1 to S phase in the cell cycle.[42] The phosphorylation state of all identified sites on RPS6 was significantly decreased, indicating an inactive state of the mTorc1 pathway.[43] RPS6 is a biomarker for drug resistance in multiple cancer types,[44] and here we show clearly that the regulation of phosphorylation status in vivo of this protein is different from the in vitro model. The inactivation of the MAPK and mTorc1 pathway in the xenograft model suggests activation of other pathways to allow for tumor growth. This activation is seen in the WNT signaling pathway and focal adhesion pathway. In the WNT signaling pathway we see increased expression of MAPK9, leading to an increase in phosphorylation of its downstream substrate CTNNB1, leading to transcriptional activation and promotion of tumor cell invasion.[45,46] The increased phosphorylation of BAD in the focal adhesion pathway inactivates the pro-apoptotic function of BAD, leading to an additional increase in survival of the tumor cells[47]

DISCUSSION

The gene-centric nature of proteomics visualization software tools hampers the ability to comprehensively map and study PTM site-centric dynamics. Here we present PhosphoPath for the visualization and analysis of quantitative proteome and phosphoproteome data sets. PhosphoPath allows the user to visualize phosphoproteomic data sets and brings knowledge in the network by importing data from three different databases or a user-defined interaction data set. It creates a network by adding protein−protein interactions and kinase−substrate interactions, and the network can be enlarged with interacting partners extracted from Biogrid and PhosphoSitePlus. Edges representing protein−protein interactions and kinase−substrate interactions are automatically added to the network, which are also added for sets of user-defined proteins. It further calculates pathway enrichment using pathway information from Wikipathways. The user can select pathways of interest for further analysis and add quantitative information on single or multiple time-points, where most tools allow for visualization of only one or two conditions. By importing quantitative information

DOI: 10.1021/acs.jproteome.5b00529
J. Proteome Res. 2015, 14, 4332−4341

on time points and integrating proteome and phosphoproteome information, pathway dynamics can be visualized over time. PhosphoPath adds several important features to existing tools for the analysis and visualization of PTM-centric data. Most importantly, PhosphoPath handles quantitative PTM data in a site-specific manner, visualizing quantification data per PTM site, unlike existing tools where PTM data is reduced in its totality to the protein level. Moreover, by extracting site-specific information from publicly available resources, one can further bring biological knowledge in the network. The added value of PhosphoPath in the analysis of PTM dynamics is exemplified by the quantitative (phospho)proteomics study of xenograft tumor growth. In this study we aimed to investigate differential phosphorylation dynamics of melanoma cells grown in either conventional cell culture or tumor xenografts and use PhosphoPath to mine the data and visualize signaling events over 3 weeks of tumor growth.

The site-specificity of PhosphoPath in combination with the addition of time series quantification facilitates the representation of phosphorylation dynamics during tumor growth. RB1 serves as a clear example, where in the first week of transplantation in the xenograft model we see a decrease in phosphorylation levels of RB1, followed by an increase in phosphorylation in weeks 2 and 3, coinciding increased tumor growth. Moreover, as described in the results, we see a decrease in activity in the MAPK pathway during melanoma xenograft growth, suggesting the activation of other signaling pathways. Because several pathways are being regulated by paracrine signaling, we would expect these pathways to be differentially regulated in the xenograft model. Because of increased activating signals from the environment, we see activation of the focal adhesion and WNT signaling pathways. The focal adhesion network shows an up-regulation of the phosphorylation state of PAK1 on multiple sites as well as for its downstream substrates BAD, BRAF, and STMN1 (Supplementary Figure S1). This increased phosphorylation leads to an inactive state of BAD, leading to interaction with 14−3−3 scaffold proteins and loss of interaction with Bcl-2. This phosphorylation state inactivates the pro-apoptotic function of BAD, leading to increased survival of the tumor cells.[47] Furthermore, the increased activation of CTNNB1 in the WNT signaling pathway, leads to transcriptional activation and promotion of tumor cell invasion.[45,46] These results indicate a decrease in MAPK activity after introduction in the xenograft model, while tumor growth is promoted by increased activation of the WNT signaling and focal adhesion pathways over time due to activating signals from the tumor environment. In summary, PhosphoPath can considerably improve the analysis of PTM-centric data by visualizing quantitative signaling dynamics in a site-specific manner. Multiple pathways can be easily visualized over time to allow for PTM-dependent analysis of signaling states. PhosphoPath is available in the Cytoscape App Store for download and can be installed in Cytoscape version 3.

■ ASSOCIATED CONTENT

Supporting Information

The Supporting Information is available free of charge on the ACS Publications website at DOI: 10.1021/acs.jproteome.5b00529. PhosphoPath and a manual with example data sets is made available at https://github.com/linseyr/PhosphoPath/ and in the Cytoscape App Store. All proteomics data has been uploaded to the Pride database; ProteomeXchange ID: PXD002599

Supplementary Figure S1. Interaction network of members of the WNT pathway. Supplementary Figure S2. Interaction network of members of the focal adhesion pathway. Supplementary Figure S3. Tandem MS spectra from singly and multiply phosphorylated peptides from the protein STMN1. Supplementary Figure S4. HE staining results. (PDF)

Supplementary Table 1. MaxQuant output ProteinGroups. (XLSX)

Supplementary Table 2. MaxQuant output phosphorylation sites. (XLSX)

■ AUTHOR INFORMATION

Corresponding Author

*Phone: +31 30 253 9554. E-mail: m.altelaar@uu.nl.

Present Address

‖P.A.P.: Division of Cell Biology, Brazilian National Cancer Institute. Rua Andre Cavalcanti, 37, 20231-050, Rio de Janeiro, Brazil.

Notes

The authors declare no competing financial interest.

■ ACKNOWLEDGMENTS

A.F.M.A. was supported by The Netherlands Organization for Scientific Research (NWO) with a VIDI grant (723.012.102) and D.S.P. was supported by a NWO VICI grant and a Queen Wilhelmina Award grant from the Dutch Cancer Society (KWF Kankerbestrijding). This work is part of the project Proteins At Work embedded in The Netherlands Proteomics Center, financed by The Netherlands Organisation for Scientific Research (NWO) as part of the National Roadmap Large-scale Research Facilities of The Netherlands (project number 184.032.201).

■ REFERENCES

(1) Zhang, H.; Zha, X.; Tan, Y.; Hornbeck, P. V.; Mastrangelo, A. J.; Alessi, D. R.; Polakiewicz, R. D.; Comb, M. J. Phosphoprotein Analysis Using Antibodies Broadly Reactive against Phosphorylated Motifs. *J. Biol. Chem.* **2002**, *277*, 39379−39387.

(2) Dephoure, N.; Gould, K. L.; Gygi, S. P.; Kellogg, D. R. Mapping and Analysis of Phosphorylation Sites: A Quick Guide for Cell Biologists. *Mol. Biol. Cell* **2013**, *24*, 535−542.

(3) Gstaiger, M.; Aebersold, R. Applying Mass Spectrometry-Based Proteomics to Genetics, Genomics and Network Biology. *Nat. Rev. Genet.* **2009**, *10*, 617−627.

(4) Altelaar, a F. M.; Munoz, J.; Heck, A. J. R. Next-Generation Proteomics: Towards an Integrative View of Proteome Dynamics. *Nat. Rev. Genet.* **2013**, *14*, 35−48.

(5) Beltran, L.; Cutillas, P. R. Advances in Phosphopeptide Enrichment Techniques for Phosphoproteomics. *Amino Acids* **2012**, *43*, 1009−1024.

(6) Lemeer, S.; Heck, A. J. The Phosphoproteomics Data Explosion. *Curr. Opin. Chem. Biol.* **2009**, *13*, 414−420.

(7) Hornbeck, P. V.; Kornhauser, J. M.; Tkachev, S.; Zhang, B.; Skrzypek, E.; Murray, B.; Latham, V.; Sullivan, M. PhosphoSitePlus: A Comprehensive Resource for Investigating the Structure and Function of Experimentally Determined Post-Translational Modifications in Man and Mouse. *Nucleic Acids Res.* **2012**, *40*, D261.

(8) Diella, F.; Cameron, S.; Gemünd, C.; Linding, R.; Via, A.; Kuster, B.; Sicheritz-Pontén, T.; Blom, N.; Gibson, T. J. Phospho.ELM: A

DOI: 10.1021/acs.jproteome.5b00529
J. Proteome Res. 2015, 14, 4332−4341

Database of Experimentally Verified Phosphorylation Sites in Eukaryotic Proteins. *BMC Bioinf.* **2004**, *5*, 79.
(9) Gnad, F.; Gunawardena, J.; Mann, M. PHOSIDA 2011: The Posttranslational Modification Database. *Nucleic Acids Res.* **2011**, *39*, D253.
(10) Zhang, M.; Li, H.; He, Y.; Sun, H.; Xia, L.; Wang, L.-S.; Sun, B.; Ma, L.; Zhang, G.; Li, J.; Li, Y.-X.; Xie, L. Construction and Deciphering of Human Phosphorylation-Mediated Signaling Transduction Networks. *J. Proteome Res.* **2015**, *14*, 150526033635001.
(11) Wu, R.; Dephoure, N.; Haas, W.; Huttlin, E. L.; Zhai, B.; Sowa, M. E.; Gygi, S. P. Correct Interpretation of Comprehensive Phosphorylation Dynamics Requires Normalization by Protein Expression Changes. *Mol. Cell. Proteomics* **2011**, *10* (8), M111.009654.
(12) Franceschini, A.; Szklarczyk, D.; Frankild, S.; Kuhn, M.; Simonovic, M.; Roth, A.; Lin, J.; Minguez, P.; Bork, P.; Von Mering, C.; Jensen, L. J. STRING v9.1: Protein-Protein Interaction Networks, with Increased Coverage and Integration. *Nucleic Acids Res.* **2013**, *41*, D808.
(13) Chatr-Aryamontri, A.; Breitkreutz, B. J.; Heinicke, S.; Boucher, L.; Winter, A.; Stark, C.; Nixon, J.; Ramage, L.; Kolas, N.; O'Donnell, L.; Reguly, T.; Breitkreutz, A.; Sellam, A.; Chen, D.; Chang, C.; Rust, J.; Livstone, M.; Oughtred, R.; Dolinski, K.; Tyers, M. The BioGRID Interaction Database: 2013 Update. *Nucleic Acids Res.* **2013**, *41*, D816.
(14) Van Iersel, M. P.; Kelder, T.; Pico, A. R.; Hanspers, K.; Coort, S.; Conklin, B. R.; Evelo, C. Presenting and Exploring Biological Pathways with PathVisio. *BMC Bioinf.* **2008**, *9*, 399.
(15) Shannon, P.; Markiel, A.; Ozier, O.; Baliga, N. S.; Wang, J. T.; Ramage, D.; Amin, N.; Schwikowski, B.; Ideker, T. Cytoscape: A Software Environment for Integrated Models of Biomolecular Interaction Networks Cytoscape: A Software Environment for Integrated Models of Biomolecular Interaction Networks. *Genome Res.* **2003**, *13*, 2498−2504.
(16) Lotia, S.; Montojo, J.; Dong, Y.; Bader, G. D.; Pico, A. R. Cytoscape App Store. *Bioinformatics* **2013**, *29*, 1350−1351.
(17) Jang, S.; Atkins, M. B. Which Drug, And When, For Patients with BRAF-Mutant Melanoma? *Lancet Oncol.* **2013**, *14*, e60−e69.
(18) Flaherty, K. T.; Puzanov, I.; Kim, K. B.; Ribas, A.; McArthur, G. A.; Sosman, J. A.; O'Dwyer, P. J.; Lee, R. J.; Grippo, J. F.; Nolop, K.; Chapman, P. B. *N. Engl. J. Med.* **2010**, *363*, 809−819.
(19) Kefford, R.; Arkenau, H.; Brown, M. P.; Millward, M.; Infante, J. R.; Long, G. V.; Ouellet, D.; Curtis, M.; Lebowitz, P. F. Phase I/II Study of GSK2118436, A Selective Inhibitor of Oncogenic Mutant BRAF Kinase, in Patients with Metastatic Melanoma and Other Solid Tumors. *J. Clin. Oncol.* **2010**, *28*, 15s (suppl; abstr 8503).
(20) Wagle, N.; Emery, C.; Berger, M. F.; Davis, M. J.; Sawyer, A.; Pochanard, P.; Kehoe, S. M.; Johannessen, C. M.; MacConaill, L. E.; Hahn, W. C.; Meyerson, M.; Garraway, L. A. Dissecting Therapeutic Resistance to RAF Inhibition in Melanoma by Tumor Genomic Profiling. *J. Clin. Oncol.* **2011**, *29*, 3085−3096.
(21) Chapman, P. B.; Hauschild, A.; Robert, C.; Haanen, J. B.; Ascierto, P.; Larkin, J.; Dummer, R.; Garbe, C.; Testori, A.; Maio, M.; Hogg, D.; Lorigan, P.; Lebbe, C.; Jouary, T.; Schadendorf, D.; Ribas, A.; O'Day, S. J.; Sosman, J. A.; Kirkwood, J. M.; Eggermont, A. M. M.; Dreno, B.; Nolop, K.; Li, J.; Nelson, B.; Hou, J.; Lee, R. J.; Flaherty, K. T.; McArthur, G. A. Improved Survival with Vemurafenib in Melanoma with BRAF V600E Mutation. *N. Engl. J. Med.* **2011**, *364*, 2507−2516.
(22) Flaherty, K. T.; Robert, C.; Hersey, P.; Nathan, P.; Garbe, C.; Milhem, M.; Demidov, L. V.; Hassel, J. C.; Rutkowski, P.; Mohr, P.; Dummer, R.; Trefzer, U.; Larkin, J. M. G.; Utikal, J.; Dreno, B.; Nyakas, M.; Middleton, M. R.; Becker, J. C.; Casey, M.; Sherman, L. J.; Wu, F. S.; Ouellet, D.; Martin, A.-M.; Patel, K.; Schadendorf, D. Improved Survival with MEK Inhibition in BRAF-Mutated Melanoma. *N. Engl. J. Med.* **2012**, *367*, 107−114.
(23) Smit, M. A.; Maddalo, G.; Greig, K.; Raaijmakers, L. M.; Possik, P. A.; van Breukelen, B.; Cappadona, S.; Heck, A. J. R.; Altelaar, A. F. M.; Peeper, D. S. *Mol. Syst. Biol.* **2014**, *10*, 772.
(24) Gillet, J.-P.; Varma, S.; Gottesman, M. M. The Clinical Relevance of Cancer Cell Lines. *J. Natl. Cancer Inst.* **2013**, *105*, 452−458.
(25) Boersema, P. J.; Raijmakers, R.; Lemeer, S.; Mohammed, S.; Heck, A. J. R. Multiplex Peptide Stable Isotope Dimethyl Labeling for Quantitative Proteomics. *Nat. Protoc.* **2009**, *4*, 484−494.
(26) Zhou, H.; Low, T. Y.; Hennrich, M. L.; van der Toorn, H.; Schwend, T.; Zou, H.; Mohammed, S.; Heck, A. J. R. Enhancing the Identification of Phosphopeptides from Putative Basophilic Kinase Substrates Using Ti (IV) Based IMAC Enrichment. *Mol. Cell. Proteomics* **2011**, *10*, M110.006452−M110.006452.
(27) Frese, C. K.; Altelaar, A. F. M.; Hennrich, M. L.; Nolting, D.; Zeller, M.; Griep-Raming, J.; Heck, A. J. R.; Mohammed, S. Improved Peptide Identification by Targeted Fragmentation Using CID, HCD and ETD on an LTQ-Orbitrap Velos. *J. Proteome Res.* **2011**, *10*, 2377−2388.
(28) Cox, J.; Mann, M. MaxQuant Enables High Peptide Identification Rates, Individualized P.p.b.-Range Mass Accuracies and Proteome-Wide Protein Quantification. *Nat. Biotechnol.* **2008**, *26*, 1367−1372.
(29) Kelder, T.; Van Iersel, M. P.; Hanspers, K.; Kutmon, M.; Conklin, B. R.; Evelo, C. T.; Pico, A. R. WikiPathways: Building Research Communities on Biological Pathways. *Nucleic Acids Res.* **2012**, *40*, D1301−D1307.
(30) Routledge, R. Fisher's Exact Test. *Encyclopedia of Biostatistics* **2005**, 1961−1964.
(31) Benjamini, Y.; Hochberg, Y. Controlling the False Discovery Rate: A Practical and Powerful Approach to Multiple Testing. *J. R. Stat. Soc. Ser. B* **1995**, *57*, 289−300.
(32) Molhoek, K. R.; Shada, A. L.; Smolkin, M.; Chowbina, S.; Papin, J.; Brautigan, D. L.; Slingluff, C. L. Comprehensive Analysis of Receptor Tyrosine Kinase Activation in Human Melanomas Reveals Autocrine Signaling through IGF-1R. *Melanoma Res.* **2011**, *21* (4), 274−284.
(33) King, C. C.; Gardiner, E. M. M.; Zenke, F. T.; Bohl, B. P.; Newton, A. C.; Hemmings, B. A.; Bokoch, G. M. p21-Activated Kinase (PAK1) Is Phosphorylated and Activated by 3-Phosphoinositide-Dependent Kinase-1 (PDK1). *J. Biol. Chem.* **2000**, *275*, 41201−41209.
(34) Ahn, S. J.; Chung, K. W.; Lee, R. A.; Park, I. A.; Lee, S. H.; Park, D. E.; Noh, D. Y. Overexpression of betaPix-a in Human Breast Cancer Tissues. *Cancer Lett.* **2003**, *193*, 99−107.
(35) Bae, J.-Y.; Ahn, S.-J.; Lee, J. E.; Kim, J.-E.; Han, M.-R.; Han, W.; Kim, S. W.; Shin, H. J.; Lee, S. J.; Park, D.; Noh, D.-Y. BetaPix-a Enhances the Activity of Phospholipase Cgamma1 by Binding SH3 Domain in Breast Cancer. *J. Cell. Biochem.* **2005**, *94*, 1010−1016.
(36) Van Aelst, L.; D'Souza-Schorey, C. Rho GTPases and Signaling Networks. *Genes Dev.* **1997**, *11*, 2295−2322.
(37) Chen, J.; Abi-Daoud, M.; Wang, A.; Yang, X.; Zhang, X.; Feilotter, H. E.; Tron, V. A. Stathmin 1 Is a Potential Novel Oncogene in Melanoma. *Oncogene* **2013**, *32*, 1330−1337.
(38) Whittaker, S. R.; Theurillat, J. P.; Van Allen, E.; Wagle, N.; Hsiao, J.; Cowley, G. S.; Schadendorf, D.; Root, D. E.; Garraway, L. A. A Genome-Scale RNA Interference Screen Implicates NF1 Loss in Resistance to RAF Inhibition. *Cancer Discovery* **2013**, *3*, 350−362.
(39) Maertens, O.; Johnson, B.; Hollstein, P.; Frederick, D. T.; Cooper, Z. A.; Messiaen, L.; Bronson, R. T.; McMahon, M.; Granter, S.; Flaherty, K.; Wargo, J. A.; Marais, R.; Cichowski, K. Elucidating Distinct Roles for NF1 in Melanomagenesis. *Cancer Discovery* **2013**, *3*, 338−349.
(40) Gibney, G. T.; Smalley, K. S. M. An Unholy Alliance: Cooperation between BRAF and NF1 in Melanoma Development and BRAF Inhibitor Resistance. *Cancer Discovery* **2013**, *3*, 260−263.
(41) Dougherty, M. K.; Müller, J.; Ritt, D. A.; Zhou, M.; Zhou, X. Z.; Copeland, T. D.; Conrads, T. P.; Veenstra, T. D.; Lu, K. P.; Morrison, D. K. Regulation of Raf-1 by Direct Feedback Phosphorylation. *Mol. Cell* **2005**, *17*, 215−224.
(42) Chakraborty, R.; Wieland, C. N.; Comfere, N. I. Molecular Targeted Therapies in Metastatic Melanoma. *Pharmacogenomics Pers. Med.* **2013**, 49−56.

DOI: 10.1021/acs.jproteome.5b00529
J. Proteome Res. 2015, 14, 4332−4341

(43) Roux, P. P.; Shahbazian, D.; Vu, H.; Holz, M. K.; Cohen, M. S.; Taunton, J.; Sonenberg, N.; Blenis, J. RAS/ERK Signaling Promotes Site-Specific Ribosomal Protein S6 Phosphorylation via RSK and Stimulates Cap-Dependent Translation. *J. Biol. Chem.* **2007**, *282*, 14056−14064.
(44) Lescarbeau, R. M.; Kaplan, D. L. Quantitative Analysis of Castration Resistant Prostate Cancer Progression through Phosphoproteome Signaling. *BMC Cancer* **2014**, *14*, 325.
(45) Fang, D.; Hawke, D.; Zheng, Y.; Xia, Y.; Meisenhelder, J.; Nika, H.; Mills, G. B.; Kobayashi, R.; Hunter, T.; Lu, Z. Phosphorylation of β-Catenin by AKT Promotes β-Catenin Transcriptional Activity. *J. Biol. Chem.* **2007**, *282* (15), 11221−11229.
(46) Van Der Velden, J. L. J.; Guala, A. S.; Leggett, S. E.; Sluimer, J.; Badura, E. C. H. L.; Janssen-Heininger, Y. M. W. Induction of a Mesenchymal Expression Program in Lung Epithelial Cells by Wingless Protein (Wnt)/β-Catenin Requires the Presence of c-Jun N-Terminal Kinase-1 (JNK1). *Am. J. Respir. Cell Mol. Biol.* **2012**, *47* (3), 306−314.
(47) Adachi, M.; Zhang, Y.-B.; Imai, K. Mutation of BAD within the BH3 Domain Impairs Its Phosphorylation-Mediated Regulation. *FEBS Lett.* **2003**, *551* (1−3), 147−152.

DOI: 10.1021/acs.jproteome.5b00529
J. Proteome Res. 2015, 14, 4332−4341